

Approaching the ultimate capacity limit in deep-space optical communication

Konrad Banaszek^{a,b}, Ludwig Kunz^{a,b}, Marcin Jarzyna^a, and Michał Jachura^{a,b}

^aCentre for Quantum Optical Technologies, University of Warsaw, Banacha 2c,
02-097 Warszawa, Poland

^bFaculty of Physics, University of Warsaw, Pasteura 5, 02-093 Warszawa, Poland

ABSTRACT

The information capacity of an optical channel under power constraints is ultimately limited by the quantum nature of transmitted signals. We discuss currently available and emerging photonic technologies whose combination can be shown theoretically to enable nearly quantum-limited operation of a noisy optical communication link in the photon-starved regime, with the information rate scaling linearly in the detected signal power. The key ingredients are quantum pulse gating to facilitate mode selectivity, photon-number-resolved direct detection, and a photon-efficient high-order modulation format such as pulse position modulation, frequency shift keying, or binary phase shift keyed Hadamard words decoded optically using structured receivers.

Keywords: Photon-starved communication, photon information efficiency, additive Gaussian noise, Holevo's bound, noise rejection, matched filter, photon counting

1. INTRODUCTION

Quantum mechanics defines the ultimate capacity limits of optical communication links.¹ In recent years, a good deal of effort has been put into devising schemes that would attain this limit in the photon-starved regime, when the propagating optical signals experience substantial attenuation bringing the number of detected photons per slot to much less than one on average.²⁻⁷ Such a regime is routinely encountered in implemented and planned optical links for transferring data collected by scientific instruments onboard deep-space missions.⁸⁻¹¹

In this contribution, we address the role of excess optical noise, which adds a random fluctuating component to the complex amplitude of the transmitted signal. Such noise originates e.g. from stray light scattering in a free-space optical channel. We point out that the excess noise defines the ultimate quantum mechanical limit on the photon information efficiency attainable in deep-space optical communication systems. Interestingly, this bound has a very weak, logarithmic dependence on the excess noise power spectral density. We discuss assumptions underlying its derivation and identify emerging photonic technologies that could make it relevant to the operation of actual deep-space optical communication links.

2. CAPACITY LIMITS

Throughout this paper we will assume that the time axis is divided into discrete slots. The duration τ of a single slot is defined by the inverse of the bandwidth B of the optical channel, $\tau = 1/B$. A convenient figure of merit is the average optical energy detected in a single slot, expressed in the units of the energy hf_c of a single photon at the carrier frequency f_c . Here $h = 6.626 \times 10^{-34}$ J·s is Planck's constant. The resulting quantity is the *average detected photon number per slot*

$$n_a = \frac{\eta P_{\text{tx}} \tau}{hf_c} = \frac{\eta P_{\text{tx}}}{Bhf_c} \quad (1)$$

where P_{tx} is the transmitter power and η is a linear factor characterizing the overall channel transmission. For notational simplicity we will take η to incorporate also the efficiency of the detection system. If in the course

Further author information: (Send correspondence to K.B.)
K.B.: E-mail: k.banaszek@cent.uw.edu.pl

of propagation the signal acquires a stochastic component generated by broadband Gaussian noise with power spectral density N_b , its contribution can be quantified using the *average number of background photons detected per slot*,

$$n_b = \frac{N_b}{\hbar f_c}. \quad (2)$$

The information capacity of an optical channel is typically analyzed under the assumption of a fixed average power. If both field quadratures are utilized to encode information and are read out via shot-noise limited heterodyne detection, the capacity per slot takes the form

$$C_{\text{het}} = \log_2 \left(1 + \frac{n_a}{1 + n_b} \right) \quad (3)$$

and the optimal constellation in the complex amplitude plane is given by a phase-invariant two-dimensional Gaussian distribution centered at zero. When information is encoded only in one field quadrature and retrieved using a homodyne receiver operating at the shot-noise limit, the capacity per slot reads

$$C_{\text{hom}} = \frac{1}{2} \log_2 \left(1 + \frac{4n_a}{1 + 2n_b} \right). \quad (4)$$

In this case the optimal constellation is one-dimensional with the Gaussian distribution for the detected quadrature and the conjugate quadrature set to zero.

Expressions given in Eq. (3) and Eq. (4) follow from the Shannon-Hartley theorem. The fractions appearing in the argument of the logarithm have the straightforward interpretation of the signal-to-noise ratio. In each case the noise term in the denominator is a sum of two contributions. The first one, equal to one owing to the choice of units made here, comes from the detection process assumed to operate at the shot noise limit.^{12,13} The second contribution stems from the excess noise added to the signal propagating through the channel. The shot noise defines natural units for the signal and the background noise strength used in definitions (1) and (2).

The ultimate quantum mechanical capacity¹⁴ is derived under the assumption that at the output of the channel one can implement the most general measurement permitted by quantum theory. We will refer to this quantity as the *Holevo capacity*. The explicit expression for the Holevo capacity in the case of a noisy channel reads:¹

$$C_{\text{Holev}} = g(n_a + n_b) - g(n_b), \quad g(x) = (x + 1) \log_2(x + 1) - x \log_2 x. \quad (5)$$

The above expression has a different mathematical form compared to Eqs. (3) and (4). Somewhat bafflingly from the perspective of the classical theory, the signal-to-noise ratio term can no longer be identified in a straightforward manner.

In the following, it will be convenient to switch to photon information efficiency (PIE) defined by $\text{PIE} = C/n_a$ as a performance measure. PIE provides the proportionality factor between the attainable information rate and the detected photon flux. Fig. 1 depicts PIE in the photon-starved regime for several values of the background noise in the range $10^{-5} \leq n_b \leq 10^{-2}$. A dramatic difference is seen in the asymptotic limit $n_a \rightarrow 0$ between the conventional coherent (heterodyne or homodyne) detection on one hand and the Holevo bound on the other hand. Analytical expressions for the asymptotic values of PIE can be easily obtained by expanding respective capacities up to the linear term in n_a , which yields:

$$\text{PIE}_{\text{het}} \rightarrow \frac{1}{1 + n_b} \log_2 e, \quad \text{PIE}_{\text{hom}} \rightarrow \frac{2}{1 + 2n_b} \log_2 e, \quad \text{PIE}_{\text{Holev}} \rightarrow \log_2 \left(1 + \frac{1}{n_b} \right). \quad (6)$$

For heterodyne and homodyne detection, PIE is upper bounded respectively by $1 \text{ nat} = \log_2 e$ and 2 nats of information. Furthermore, as long as $n_b \ll 1$ the background noise plays a negligible role, being dominated by the detection shot noise which remains at a constant level. In contrast, the Holevo bound for PIE depends dramatically on the background noise strength. In the regime $n_b \ll 1$ it exhibits a simple logarithmic dependence $\text{PIE}_{\text{Holev}} \sim \log_2(1/n_b)$. For example, $n_b = 10^{-3}$ sets the effective upper bound on PIE slightly at less than 10 bits per photon. Based on Fig. 1 one can infer a simple rule of thumb that the asymptotic value of the Holevo PIE bound is reached when the signal strength n_a becomes lower than the background noise strength, i.e. $n_a \lesssim n_b$.

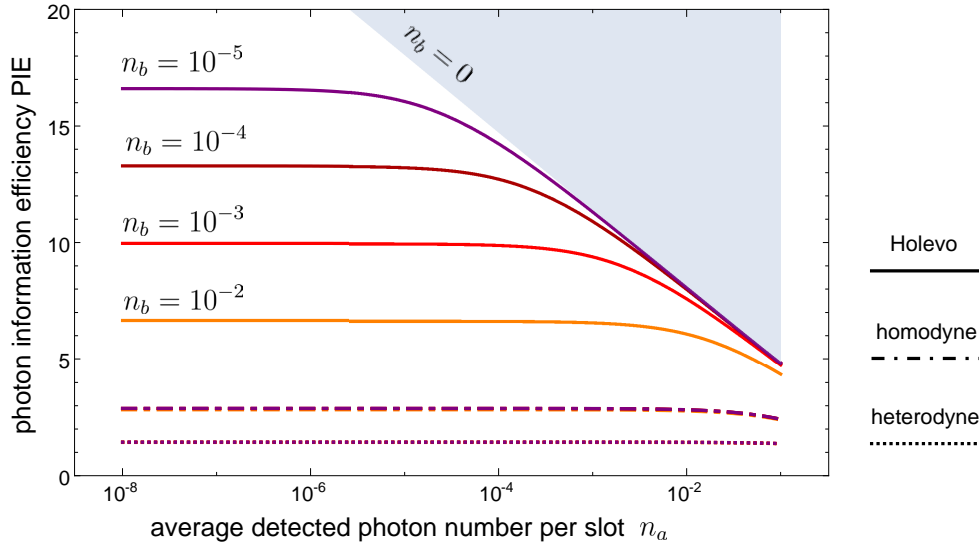


Figure 1. Capacity limits in photon-starved communication shown as a dependence of the photon information efficiency PIE on the average number of detected photons per slot for several values of the background noise strength $n_b = 10^{-5}, 10^{-4}, 10^{-3}$, and 10^{-2} . Solid lines depict the Holevo bound, while overlapping sets dotted and dash-dotted lines correspond respectively to heterodyne and homodyne capacities. The edge of the shaded area indicates the noiseless Holevo bound given by $g(n_a)$ as specified in Eq. (5).

3. NOISE REJECTION

It is illuminating to discuss in more detail the noise model underlying the capacity limits presented in the preceding section. The optical field emerging from a noisy channel, shown schematically in Fig. 2(a), carries information in the complex amplitude α of a certain normalized signal mode (waveform) characterized by its envelope $u_0(t)$. Consider broadband additive Gaussian excess noise, visualized in Fig. 2(a) as a semi-transparent strip overlaid on the signal waveform. The noise can be decomposed in an basis orthonormal of modes $u_0(t), u_1(t), u_2(t), \dots$ shown in Fig. 2(a), chosen such that the first mode $u_0(t)$ is identical with the signal mode. Thus the signal mode carries the modulated amplitude plus the noise contribution, while all the other modes contain only the background noise. A single realization of the field can be written as $\mathcal{E}(t) \exp(-2\pi i f_c t)$ with the envelope given by a sum

$$\mathcal{E}(t) \propto (\alpha + \beta_0)u_0(t) + \beta_1 u_1(t) + \beta_2 u_2(t) + \dots \quad (7)$$

We will choose the units for the complex amplitudes multiplying mode functions such that their squared absolute values specify the average numbers of photons in individual modes. For broadband noise, the stochastic amplitudes $\beta_0, \beta_1, \beta_2, \dots$ are characterized by the same phase-invariant Gaussian distribution with a zero mean, the second moment equal to

$$\langle |\beta_0|^2 \rangle = \langle |\beta_1|^2 \rangle = \langle |\beta_2|^2 \rangle = \dots = n_b, \quad (8)$$

and lack of correlations, $\langle \beta_i \beta_j \rangle = \langle \beta_i \beta_j^* \rangle = 0$ for $i \neq j$.

Expressions for channel capacities presented in Eqs. (3)–(5) are derived assuming that $\langle |\alpha|^2 \rangle = n_a$ and that only the noise present in the signal mode $u_0(t)$ is taken into account, while contributions from modes $u_1(t), u_2(t), \dots$ are rejected. This assumption is naturally satisfied for coherent detection, which measures only the amplitude of a specific waveform matching the temporal shape of the local oscillator.¹⁵ Alternatively, the detected mode can be defined in digital signal postprocessing if the detector electronic output is sampled at a sufficiently high rate. On the other hand, the applicability of such a model to the direct detection scenario requires a more careful inspection.

According to the photodetection theory,¹⁶ the photocount statistics is a function of the optical power $|\mathcal{E}(t)|^2$ time-integrated over the detection window. Clearly, with $\mathcal{E}(t)$ given by Eq. (7) such an integral will contain

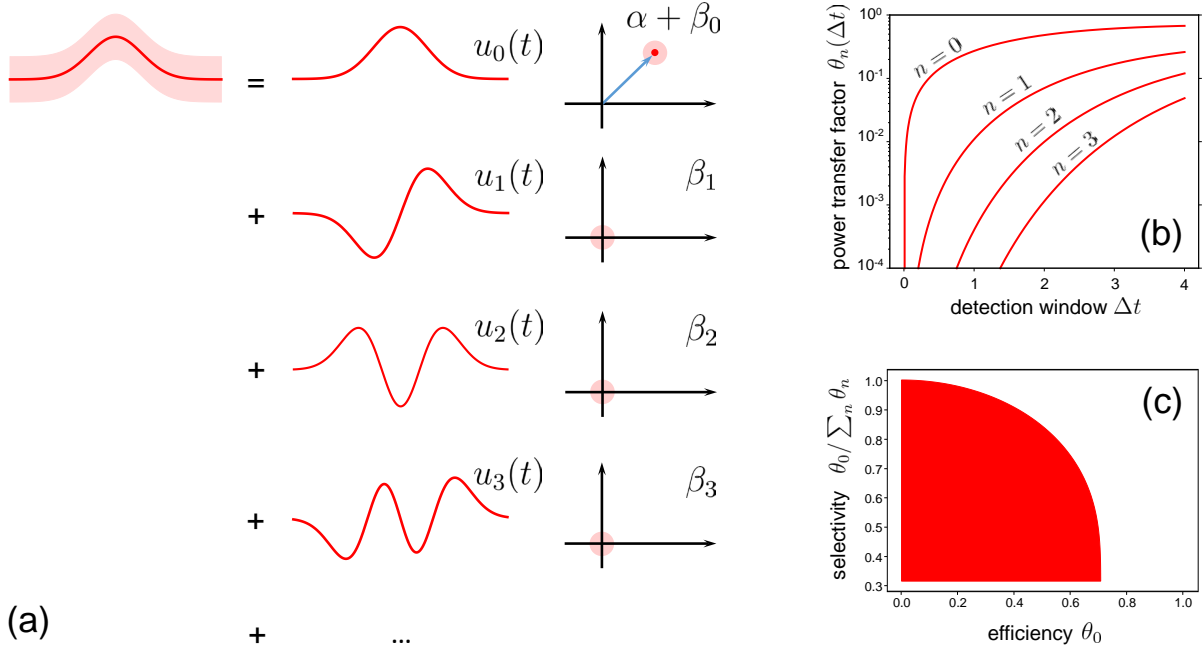


Figure 2. (a) Noisy signal field can be decomposed in a basis of temporal modes. The waveform $u_0(t)$ carrying information in the complex amplitude α is complemented with orthogonal modes $u_1(t), u_2(t), u_3(t), \dots$. The noise contributes random complex amplitudes β_0, β_1, \dots to individual modes. (b) The power transfer coefficients $\theta_n(\Delta t)$ for Gauss-Hermite modes $u_n(t)$ as a function of the detection window Δt with the matched filter implemented optically in the form of spectral optical filtering with peak transmission equal to one. (c) The resulting trade-off between the filter efficiency θ_0 and the selectivity $\theta_0 / \sum_{n=0}^{\infty} \theta_n$ with the accessible values shown as the solid red area.

contributions not only from the mode $u_0(t)$, but also from other modes $u_1(t), u_2(t), \dots$. In principle, the contribution to the optical field from the signal mode $u_0(t)$ in Eq. (7) can be separated using the *matched filter*¹⁷ $f(t) \propto u_0^*(-t)$ such that the convolution

$$(f \star \mathcal{E})(t) = \int_{-\infty}^{\infty} dt' f(t-t') \mathcal{E}(t') \quad (9)$$

yields $(f \star \mathcal{E})(0) \propto \alpha + \beta_0$ at time $t = 0$. Optically, convolution in the temporal domain can be realized by sending the signal through a spectral filter with the amplitude transfer function given by the Fourier transform of $f(t)$. Detecting subsequently the output field over a short time window centered at $t = 0$ would provide response dependent only on the amplitude $\alpha + \beta_0$ of the signal mode. However, the basic drawback of this scheme is the loss of the signal power. This can be seen most easily by inspecting the effective power transfer coefficients $\theta_n(\Delta t)$ that specify how much optical power from individual modes $u_n(t)$ contributes to the detection window of duration Δt :

$$\theta_n(\Delta t) = \int_{-\Delta t/2}^{\Delta t/2} dt |(f \star u_n)(t)|^2. \quad (10)$$

Fig. 2(b) shows the coefficients $\theta_n(\Delta t)$ assuming Gauss-Hermite modes $u_n(t) = H_n(t)e^{-t^2/2}/(\pi^{1/2}2^n n!)^{1/2}$ and unit peak transmission of the spectral filter. It is seen that while the selectivity improves with shorter time windows Δt , the efficiency of selecting the signal component drops significantly below 100%. Importantly, even for long time windows Δt the power transfer is limited to slightly below 71%. The resulting trade-off between the efficiency θ_0 and the selectivity $\theta_0 / \sum_{n=0}^{\infty} \theta_n$ is depicted in Fig. 2(c).

The capacity limits defined in Eqs. (3)–(5) involve an absolute, input-independent scale for the signal and noise strengths. This scale is defined by the detector shot-noise level in the case of coherent detection, or more

fundamentally by the granular nature of electromagnetic radiation taken into account in the Holevo bound. Consequently, to approach the capacity limit it would be necessary to pick up the signal mode with 100% efficiency *and* 100% selectivity.

Deficiencies of conventional spectral filtering described above are in principle absent in the recently introduced technique of quantum pulse gating.^{18,19} The basic idea is to select from a composite field, such as the one given in Eq. (7), a single temporal mode with 100% efficiency in a way that does not alter its quantum statistical properties. Such a quantum pulse gate (QPG) can be implemented using three-wave mixing in a $\chi^{(2)}$ nonlinear medium with carefully engineered phase matching properties. The composite field is sent into the medium along with an auxiliary pulse so that sum-frequency generation takes place only between the mode of interest and the auxiliary pulse mode. At the output of the medium the frequency-upconverted mode is separated spectrally, using e.g. a dichroic mirror, from the remaining field. In a proof-of-principle demonstration with near-infrared ultrashort sub-picosecond pulses,²⁰ conversion efficiency exceeding 80% for the Gauss-Hermite signal mode $u_0(t)$ has been achieved with less than 20% power transferred for the first-order mismatched mode $u_1(t)$. While theoretical limits on the conversion efficiency in a single-stage QPG have been indicated, the coherent nature of the sum-frequency generation process allows one to overcome them by cascading two or more QPGs with individual conversion efficiencies lower than one.^{21,22} It is worth to mention also other functionality of quantum pulse gating, such as changing the bandwidth of the gated signal²³ and converting the carrier frequency to the spectral range where more efficient photon counting is available.

4. PULSE POSITION MODULATION

The standard strategy to achieve high PIE in photon-starved optical communication is to employ the pulse position modulation (PPM) format with direct detection. Photon counting as a detection technique goes beyond the measurement of field quadratures, which makes void capacity limits resulting from the application of the Shannon-Hartley theorem to readout based on conventional coherent detection.

In a typical ground receiver setup for downlink transmission the photon counting detector responds to radiation present in multiple temporal and spatial modes. In the temporal degree of freedom, the effective number of modes is roughly given the product of the slot duration and the bandwidth of the spectral filter used to suppress the background noise outside the signal spectrum.²⁴ In the spatial degree of freedom, atmospheric turbulence distorts the signal wavefront well beyond the diffraction limit. The distorted wavefront needs to be accommodated with a sufficiently large active area of the detector that consequently becomes sensitive to background radiation present in spatial modes other than the signal one. When background counts are generated by noise contributions from a large number of weakly excited modes, their statistics can be modelled by a Poissonian distribution. The PPM limits for such a multimode noise model, assuming a photon counting detector operated in the Geiger mode, i.e. providing a binary response whether at least one photon has been detected in a given slot or none at all, have been recently analyzed by Zwoliński *at al.*²⁵ The basic conclusion is that for a fixed background noise level one can in principle achieve non-zero photon information efficiency in the limit of a diminishing signal strength. The prerequisites are complete decoding to recover information from all sequences of photocounts that may occur within individual PPM frames and sufficient concentration of optical energy in signal pulses, which should contain between ~ 0.2 and ~ 1.1 photon at the detection stage for noise strengths ranging from 10^{-5} to 10^{-1} background counts per slot.²⁶

Obviously, the multimode noise model cannot be directly compared with the Holevo capacity bound. From the theoretical viewpoint, background noise present in modes other than the signal mode can be rejected without affecting the signal itself and therefore it does not fundamentally limit the link capacity. Although achieving in practice single-mode direct detection of the signal waveform would be challenging, it may no longer seem totally outlandish on the second thought. Adaptive optics technology enables compensation of wavefront distortion effects and could facilitate delivery of the received signal to the detection stage in a single spatial mode. Further, as discussed in Sec. 3, the technique of quantum pulse gating provides in principle means to pick up the temporal signal mode with nearly 100% efficiency and very good selectivity.

Given the above motivation, it is interesting to examine the efficiency of a PPM link assuming the single-mode model for the background noise. In this scenario, the probabilities of registering k photocounts on a photon

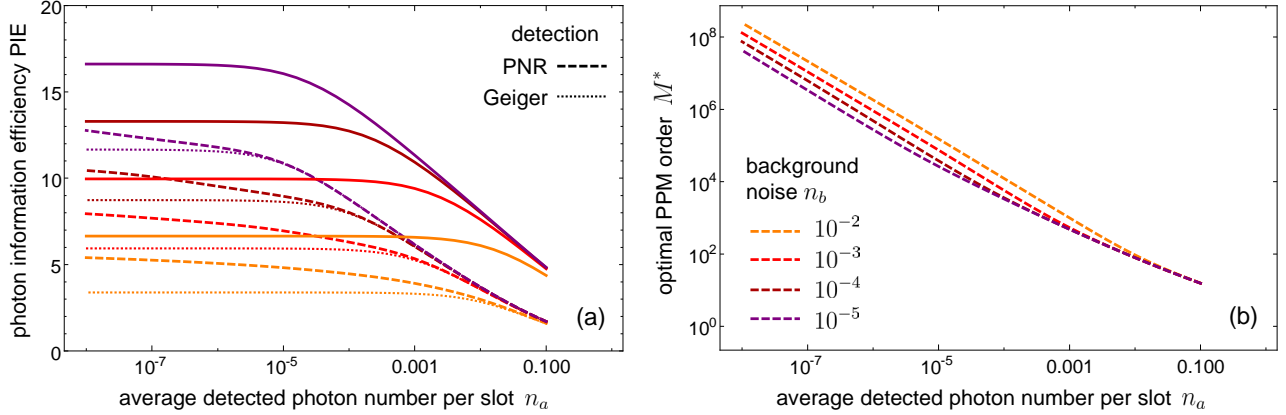


Figure 3. (a) Photon information efficiency for the PPM format as a function of the average detected photon number n_a optimized in the case of photon number resolved (dashed lines) and Geiger-mode (thin dotted lines) detection. For reference, solid lines depict the Holevo bound. (b) Optimal PPM orders for photon number resolved detection as a function of the signal strength.

number resolving detector respectively for an empty slot “0” and a pulse “1” are given by:²⁷

$$p_0(k) = \frac{n_b^k}{(1+n_b)^{k+1}}, \quad p_1(k) = \frac{n_b^k}{(1+n_b)^{k+1}} \exp\left(-\frac{Mn_a}{1+n_b}\right) L_k\left(-\frac{Mn_a}{n_b(1+n_b)}\right). \quad (11)$$

Here M is the PPM order and $L_k(\cdot)$ denotes the k th Laguerre polynomial. For a given average detected signal photon number n_a and the background noise strength n_b optimization has been carried out over the PPM order M taking as the cost function a lower bound on the PPM efficiency based on relative entropy. Two types of direct detection have been considered: photon number resolved (PNR) detection, which gives the actual photocount number k , and Geiger-mode detection, which discriminates only between $k = 0$ and $k \geq 1$.

Fig. 3(a) depicts results of optimization for background noise strengths $n_b = 10^{-5}, 10^{-4}, 10^{-3}$, and 10^{-2} . The most interesting feature is that for PNR detection the gap between the optimized PPM photon information efficiency and the Holevo bound closes with diminishing signal strength. Indeed, it can be shown mathematically that the capacity per unit cost for PPM with PNR detection approaches the Holevo limit.²⁸ Photon number resolving capability is essential here: it is seen that for Geiger-mode detection the attainable PIE stays below the Holevo bound. This result is in a stark contrast with the noiseless ($n_b = 0$) scenario, where a double-logarithmic gap opens up with the diminishing signal strength between optimized PPM PIE and the Holevo bound.^{29–31}

5. OUTLOOK

Achieving information efficiency identified in the preceding section requires implementation of the PPM format with very high orders, as shown in Fig. 3(b). Basically, the pulses should be bright enough to generate several photocounts on the detector to facilitate robust discrimination against background counts. This detection regime resembles that employed recently in low-intensity LiDAR technology,³² where the light intensity in the few-photon range also needs to be measured within a short time window. Another prerequisite to approach the Holevo limit is soft-decoding of the receiver output with efficiency attaining the Shannon information limit, which is implicitly assumed in the relative-entropy bound used in numerical calculations.

The principal technological challenge on the transmitter side to produce a high-order PPM signal is the high peak-to-average power ratio of the laser source. This obstacle could be removed by switching to one of other high-order modulation formats visualized using time-frequency diagrams presented in Fig. 4 that are capable of delivering equivalent information efficiency.³³ In the case of the PPM format depicted in Fig. 4(a), the modulation bandwidth B defines the length τ of a single slot in the time domain as $\tau = B^{-1}$. Therefore one M -ary PPM symbol has duration $M\tau = MB^{-1}$, covers the area MB^{-1} (time) $\times B$ (frequency), and carries

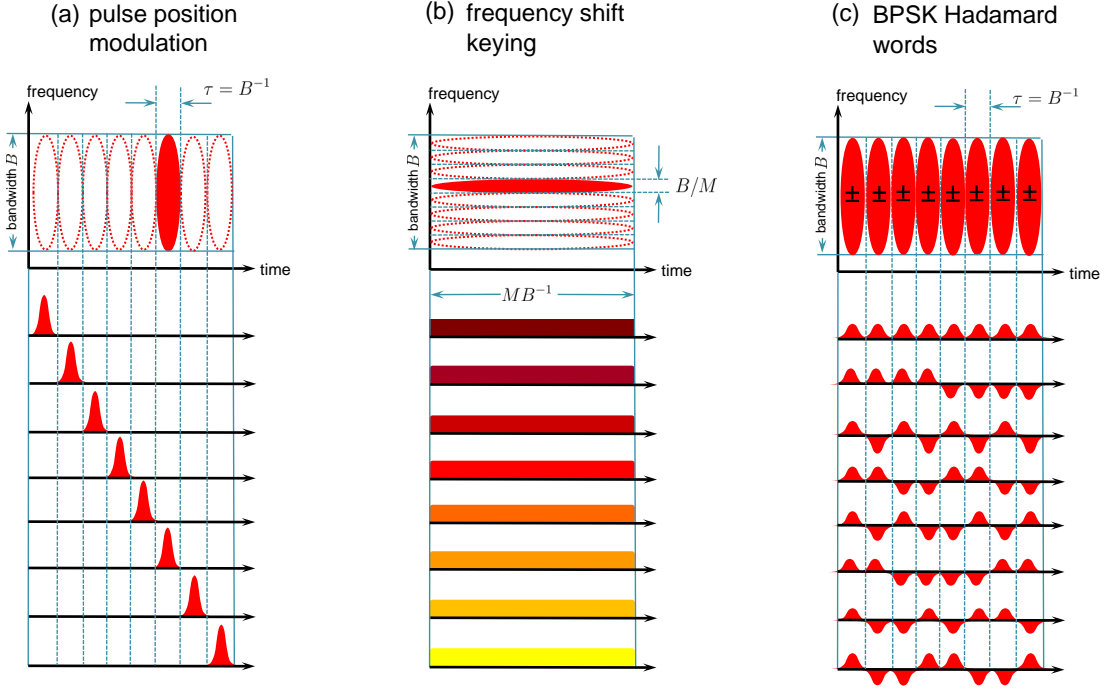


Figure 4. Time-frequency diagrams for (a) pulse position modulation, (b) frequency shift keying, and (c) Hadamard words composed from the BPSK alphabet shown for the format order $M = 8$. In all three cases individual symbols occupy the same $MB^{-1} \times B$ area in the time-frequency plane and are characterized by the optical energy Mn_a .

optical energy Mn_a measured at the detection stage. As illustrated in Fig. 4(b), the same time-frequency area can be sliced in the spectral domain into M frequency slots, each of spectral width B/M and temporal duration MB^{-1} , which yields the frequency shift keying (FSK) modulation format. The optical energy Mn_a of each symbol is now spread evenly across the entire time frame. In the context of free-space optical communication, scalable FSK modulation has been demonstrated by selecting individual spectral lines from a frequency comb using a sequence of electrooptically controlled Mach-Zehnder interferometric filters.³⁴ On the other hand, the readout of FSK symbols would require a high-resolution, low-loss spectrometer followed by an array of photon counting detectors.

Yet another option to prepare M symbols covering the $MB^{-1} \times B$ time-frequency area with a uniform distribution of instantaneous power is to generate sequences of binary phase shift keyed (BPSK) pulses in M consecutive time slots, as shown in Fig. 4(c). When signs for BPSK sequences are taken as rows of Hadamard matrices, it is possible to convert all-optically received pulse trains into the PPM format using structured receivers that implement optical interference between multiple time slots.³ Importantly, scalable designs for structured optical receivers have been presented.³⁵ A major advantage of the modulation format based on such BPSK Hadamard words is that pulse sequences could be generated by a transmitter based on standard telecom components. Furthermore, the modulation order M is software-defined in the encoding layer of the communication system and changing it does not require any hardware adjustments. The main challenge of implementing this modulation format would be the construction of a reliable structured optical receiver. Elements of the required technology are shared with other setups for free-space optical communication, such as links utilizing the differential phase shift keying (DPSK) format³⁶ and quantum key distribution based on time-bin qubit encoding.³⁷ Looking at less mature technologies, the BPSK signal might be a good candidate to implement noise rejection using the quantum pulse gating technique, provided that temporal synchronization with the receiver setup can be established.

ACKNOWLEDGMENTS

We acknowledge insightful discussions with C. Antonelli, H. Eisenberg, A. Mecozzi, and M. Shtaif. This work is part of the project “Quantum Optical Communication Systems” carried out within the TEAM programme of the Foundation for Polish Science co-financed by the European Union under the European Regional Development Fund.

REFERENCES

- [1] Giovannetti, V., García-Patrón, R., Cerf, N. J., and Holevo, A. S., “Ultimate classical communication rates of quantum optical channels,” *Nature Photon.* **8**, 796–800 (2014).
- [2] Erkmén, B. I., Moision, B. E., and Birnbaum, K. M., “A review of the information capacity of single-mode free-space optical communication,” in [*Free-Space Laser Communication Technologies XXII*], Hemmati, H., ed., **7587**, 75870N, SPIE (2010).
- [3] Guha, S., “Structured optical receivers to attain superadditive capacity and the Holevo limit,” *Phys. Rev. Lett.* **106**(24), 240502 (2011).
- [4] Erkmén, B. I., Moision, B. E., Dolinar, S. J., Birnbaum, K. M., and Divsalar, D., “On approaching the ultimate limits of communication using a photon-counting detector,” in [*Free-Space Laser Communication Technologies XXIV*], **8246**, 824605, SPIE (2012).
- [5] Takeoka, M. and Guha, S., “Capacity of optical communication in loss and noise with general quantum gaussian receivers,” *Phys. Rev. A* **89**(4), 042309 (2014).
- [6] Rosati, M., Mari, A., and Giovannetti, V., “Multiphase Hadamard receivers for classical communication on lossy bosonic channels,” *Phys. Rev. A* **94**(6), 062325 (2016).
- [7] Chung, H. W., Guha, S., and Zheng, L., “Capacity of optical communications over a lossy bosonic channel with a receiver employing the most general coherent electro-optic feedback control,” *Phys. Rev. A* **96**(1), 012320 (2017).
- [8] Hemmati, H., Biswas, A., and Djordjevic, I. B., “Deep-space optical communications: Future perspectives and applications,” *Proc. IEEE* **99**(11), 2020–2039 (2011).
- [9] Moision, B. and Farr, W., “Range dependence of the optical communications channel,” *IPN Prog. Rep.* **42-199**, 1–10 (2014).
- [10] Boroson, D. M., “On achieving high performance optical communications from very deep space,” in [*Free-Space Laser Communication and Atmospheric Propagation XXX*], Hemmati, H. and Boroson, D. M., eds., **10524**, 105240B, SPIE (2018).
- [11] Arapoglou, P.-D., Sodnik, Z., Heese, C., Schulz, K.-J., Zayer, I., and Daddato, R. J., “European deep-space optical communications program,” in [*Free-Space Laser Communication and Atmospheric Propagation XXX*], Hemmati, H. and Boroson, D. M., eds., **10524**, 105240Q, SPIE (2018).
- [12] Yuen, H. P. and Chan, V. W. S., “Noise in homodyne and heterodyne detection,” *Opt. Lett.* **8**(3), 177–179 (1983).
- [13] Yuen, H. P. and Chan, V. W. S., “Noise in homodyne and heterodyne detection: errata,” *Opt. Lett.* **8**(6), 345 (1983).
- [14] Holevo, A. S., “Bounds for the quantity of information transmitted by a quantum communication channel,” *Problems of Information Transmission* **9**(3), 177–183 (1973).
- [15] Yuen, H. and Shapiro, J., “Optical communication with two-photon coherent states—part III: Quantum measurements realizable with photoemissive detectors,” *IEEE Trans. Inf. Theory* **26**(1), 78–92 (1980).
- [16] Mandel, L. and Wolf, E., [*Optical Coherence and Quantum Optics*], ch. 9, Cambridge University (1995).
- [17] Lapidot, A., [*A Foundation in Digital Communication*], Cambridge University Press, 2 ed. (2017).
- [18] Eckstein, A., Brecht, B., and Silberhorn, C., “A quantum pulse gate based on spectrally engineered sum frequency generation,” *Opt. Express* **19**(15), 13770–13778 (2011).
- [19] Brecht, B., Reddy, D. V., Silberhorn, C., and Raymer, M. G., “Photon temporal modes: A complete framework for quantum information science,” *Phys. Rev. X* **5**(4), 041017 (2015).
- [20] Reddy, D. V. and Raymer, M. G., “Engineering temporal-mode-selective frequency conversion in nonlinear optical waveguides: from theory to experiment,” *Opt. Express* **25**(11), 12952–12966 (2017).

- [21] Reddy, D. V., Raymer, M. G., and McKinstrie, C. J., “Efficient sorting of quantum-optical wave packets by temporal-mode interferometry,” *Opt. Lett.* **39**(10), 2924–2927 (2014).
- [22] Reddy, D. V. and Raymer, M. G., “High-selectivity quantum pulse gating of photonic temporal modes using all-optical Ramsey interferometry,” *Optica* **5**(4), 423–428 (2018).
- [23] Allgaier, M., Ansari, V., Sansoni, L., Eigner, C., Quiring, V., Ricken, R., Harder, G., Brecht, B., and Silberhorn, C., “Highly efficient frequency conversion with bandwidth compression of quantum light,” *Nature Commun.* **8**, 14288 (2017).
- [24] Landau, H. J. and Pollak, H. O., “Prolate spheroidal wave functions, Fourier analysis and uncertainty — III: The dimension of the space of essentially time- and band-limited signals,” *Bell Syst. Tech. J.* **41**(4), 1295–1336 (1962).
- [25] Zwoliński, W., Jarzyna, M., and Banaszek, K., “Range dependence of an optical pulse position modulation link in the presence of background noise,” *Opt. Express* **26**(20), 25827–25838 (2018).
- [26] Jarzyna, M., Zwoliński, W., and Banaszek, K., “Range dependence of pulse position modulation in the presence of background noise,” in [*International Conference on Space Optics*], SPIE (2018).
- [27] Arecchi, F., Berne, A., Sona, A., and Burlamacchi, P., “Photocount distributions and field statistics,” *IEEE J. Quantum Electron.* **2**(9), 341–350 (1966).
- [28] Jarzyna, M. private communication (2019).
- [29] Kochman, Y., Wang, L., and Wornell, G. W., “Toward photon-efficient key distribution over optical channels,” *IEEE Trans. Inf. Theory* **60**(8), 4958–4972 (2014).
- [30] Jarzyna, M., Kuszaj, P., and Banaszek, K., “Incoherent on-off keying with classical and non-classical light,” *Opt. Express* **23**(3), 3170–3175 (2015).
- [31] Jarzyna, M. and Banaszek, K., “Efficiency of optimized pulse position modulation with noisy direct detection,” in [*Proceedings of the IEEE International Conference on Satellite Optical Systems and Applications (ICSOS)*], 176–181 (2017).
- [32] Eisenberg, H., Sher, Y., Cohen, L., and Istrati, D., “Low intensity LiDAR using compressed sensing and a photon number resolving detector,” in [*Emerging Digital Micromirror Device Based Systems and Applications X*], Douglass, M. R. and Lee, B. L., eds., **10546**, 105460J, SPIE (2018).
- [33] Banaszek, K., Jachura, M., and Wasilewski, W., “Utilizing time-bandwidth space for efficient deep-space communication,” in [*International Conference on Space Optics*], SPIE (2018).
- [34] Savage, S. J., Robinson, B. S., Caplan, D. O., Carney, J. J., Boroson, D. M., Hakimi, F., Hamilton, S. A., Moores, J. D., and Albota, M. A., “Scalable modulator for frequency shift keying in free space optical communications,” *Opt. Express* **21**(3), 3342–3353 (2013).
- [35] Banaszek, K. and Jachura, M., “Structured optical receivers for efficient deep-space communication,” in [*Proceedings of the IEEE International Conference on Satellite Optical Systems and Applications (ICSOS)*], 34–37 (2017).
- [36] Sodnik, Z. and Sans, M., “Extending EDRS to laser communication from space to ground,” in [*International Conference on Space Optical Systems and Applications (ICSOS)*], (2012).
- [37] Jin, J., Agne, S., Bourgoïn, J.-P., Zhang, Y., Lütkenhaus, N., and Jennewein, T., “Demonstration of analyzers for multimode photonic time-bin qubits,” *Phys. Rev. A* **97**(4), 043847 (2018).